Analyst

Accepted Manuscript

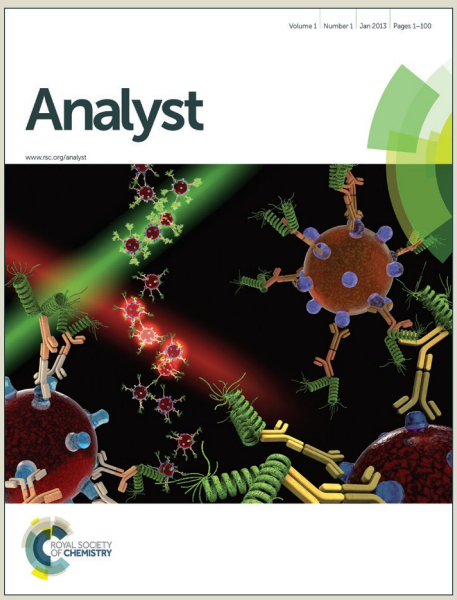

ROYAL SOCIETY OF CHEMISTRY

www.rsc.org/analyst

Simultaneous acquisition of infrared, fluorescence and light scattering spectra of proteins: direct evidence for pre-fibrillar species in amyloid fibril formation

Maurizio Baldassarre[1], Matthew Bennett and Andreas Barth
Department of Biochemistry and Biophysics, Stockholm University, Stockholm, Sweden

Keywords: Amyloid fibrils; Fourier-transform infrared spectroscopy; Thioflavin T; Fluorescence spectroscopy; light scattering; β-lactoglobulin.

Abbreviations used: βLG, β-lactoglobulin; ThT, Thioflavin T; DLS, dynamic light scattering; TEM, transmission electron microscopy; AFM, atomic force microscopy.

Abstract

Different spectroscopic approaches are often used to probe specific aspects of amyloid fibril formation but are usually performed separately and under different conditions. This makes it problematic to relate different aspects of the aggregation process when these are monitored by different methods. We report on a multispectral approach for simultaneous acquisition of infrared, fluorescence and light scattering spectra of proteins undergoing aggregation. We have applied our approach to study β-lactoglobulin, a milk protein known to form amyloid fibrils under well established conditions. Our real-time multispectral measurements show that unfolding of this protein is followed by formation of early aggregates consisting of intermolecular β-sheets with a typical infrared absorption at $\sim$1619 cm^{-1} in ^2H_2O. These aggregates, which lead to an increase in the light scattering signal, do not bind the amyloid-specific fluorophore ThT and therefore consist of oligomers or protofibrils. Fibril growth is then observed as a sigmoidal increase in ThT fluorescence. After $\sim$25 h, a plateau is observed in the intensities of ThT emission and of the band at 1619 cm^{-1}, indicating that no new fibrils are forming. However, a second phase in the light scattering signal taking place after $\sim$25 h suggests that the fibrils are assembling into larger structures, known as *mature* fibrils. This is associated with an upshift of the main β-sheet band in the infrared spectrum. TEM analyses confirmed the existence of thick fibrils comprising 3–5 filaments.

[1]**Corresponding author**: *maurizio.baldassarre@dbb.su.se*.

1 Introduction

Protein aggregation is a complex and poorly understood phenomenon in biology,[1,2] despite having enormous implications in medicine[3,4] as well as in the food[5,6] and pharmaceutical industries.[7,8] Aggregation of soluble proteins most often arises from partial or total destabilisation of their native, three-dimensional structures, leading to exposure of hydrophobic regions normally buried within the protein core.[9–11] Thermodynamic effects then push these regions together, often leading to formation of new secondary structures (intermolecular β-sheets) and supermolecular assemblies. Causes destabilising the native fold include chemical or physical agents, such as denaturants or heat, or may be the result of amino acid mutations with a destabilising effect. An example of the latter case is a pathological condition known as sickle-cell anaemia,[12,13] where a mutation from glutamate to valine, originating from a single base substitution in the β-globin gene, drives the self-assembly of haemoglobin chains into fibrous structures several μm in length.

Protein aggregation *in vivo* can have inauspicious prognoses, as in a number of degenerative pathologies clustered under the name of *amyloidoses*, *amyloid diseases* or *misfolding diseases*.[14–16] In these types of disorders, specific proteins or peptides polymerise into long structures known as amyloid (litterally *starch-like*) fibrils. Unlike amorphous aggregates, amyloid fibrils feature an ordered and repetitive molecular architecture known as cross-β structure, in which β-strands from distinct protein/peptide chains associate to form an extended, intermolecular β-sheet with a parallel or antiparallel arrangement.[17–20] Amyloid fibrils deposited inside or outside the cell can disrupt the physiological cellular activities and induce cell death. In some cases, the causative agents are small, transient assemblies (oligomers) formed on-pathway to fibril growth.[21,22]

Nowadays, it is widely accepted that virtually many polypeptide chains can be induced to form amyloid fibrils. Nevertheless, the number of amyloid diseases identified so far is relatively limited ($\sim$40).[14] What catalyses the attention of enormous medical and pharmaceutical research initiatives is the widespread occurrence, symptomatology and societal significance of some of these diseases. Notable members of the amyloid disease family include **Alzheimer's disease**[23] (causative agent: amyloid-β peptide), **Parkinson's disease**[24] (α-synuclein), **Huntington's disease**[25] (huntingtin), **diabetes mellitus type 2**[26] (amylin), **atherosclerosis**[27] (apolipoprotein AI) and **amyotrophic lateral sclerosis**[28] (superoxide dismutase 1), only to name a few examples. Alzheimer's disease alone affects almost 50 million people worldwide (data from Alzheimer's Disease International, `http://www.alzheimers.net/resources/alzheimers-statistics/`). This number is expected to triple by the year 2050. Research on amyloid formation of these proteins is an important contribution to understand and treat such amyloidoses. It aims to elucidate several aspects of these peculiar protein assemblies, such as structure, stabilities and kinetics, with the goal to slow down or reverse the process.

Infrared spectroscopy is an invaluable tool in the study of amyloid fibrils[29–33] and other protein aggregates.[1,34–37] It allows the detection of local or global structural changes in proteins and is particularly sensitive to the β-sheet.[38–41] Unlike circular dichroism, it allows for

the discrimination of parallel and antiparallel β-sheets for flat, extended sheets.[40,42] This is of particular relevance in research on Alzheimer's disease, since pre-fibrillar oligomers and mature fibrils are respectively composed of antiparallel and parallel β-sheets.[42,43]

Infrared spectroscopy, however, does not always permit to discriminate between amyloid fibrils and other aggregates, since both give rise to similar spectral signature in the amide I' region (a low-frequency β-sheet band below 1625 cm^{-1} and, in the case of antiparallel β-sheets, a weaker high-frequency component between 1695 and 1680 cm^{-1}). This type of discrimination is routinely performed by exploiting the tinctorial (*i.e.* dye-binding) properties of amyloid fibrils. Thioflavin T (ThT), for instance, is a benzothiazole fluorophore that is thought to intercalate between the rigid and regularly-spaced crevices of the cross-β structure (the exact mechanism of binding is still debated).[44,45] ThT is relatively non-fluorescent in water, but its quantum yield increases several fold upon binding to amyloid fibrils due to the rigid anisotropic environment that they provide.[46] One of the main advantages of ThT is that it can be used in continuous kinetic experiments, thereby providing real-time details on the process of fibril formation. The presence of a lag phase, for instance, indicates formation of intermediate species (such as oligomers) and suggests a nucleation-dependent mechanism for the polymerisation process.[47]

ThT can conveniently monitor formation of fibrils but it cannot provide details on the size of the aggregates in the sample. Fibril formation can be regarded as a hierarchical process in which single fibrils can bundle to form even larger assemblies, often referred to as *mature* fibrils. Other spectroscopic approaches, such as light scattering techniques, can be used to monitor changes in the mean size of the aggregates.[48] Light scattering is based on the observation that the combined magnitude of the scattering effect of two individual particles ($2\times$P) is weaker than that of a larger particle with twice their size (P_2).

In the laboratory, infrared spectroscopy, fluorescence spectroscopy and light scattering are usually not performed on the same sample since they require very different concentration ranges, different cuvettes and, more importantly, specific instruments. This prevents researchers from establishing a straightforward connection between structural or conformational changes (probed by infrared spectroscopy), nature of the aggregates (probed by ThT fluorescence) and changes in the size of the latter (probed by light scattering). A system for combined infrared and fluorescence measurements was described more than twenty years ago,[49] while one that combines infrared and light scattering has been described very recently.[50] We hereby report on the development of an integrated system for simultaneous acquisition of infrared, fluorescence and light scattering spectra of proteins undergoing aggregation. This system is shown schematically in Fig. 1 and is described in greater detail throughout the text.

The present study demonstrates the potential of our system using β-lactoglobulin (βLG) from bovine milk, a much studied amyloidogenic proteins.[51–53] The use of βLG offers several advantages. It readily forms amyloid fibrils under well established and reproducible conditions (low pH, high temperature). Several stages of aggregation have been identified, but these have been investigated separately.[54,55] This makes it ideal as a test system to examine

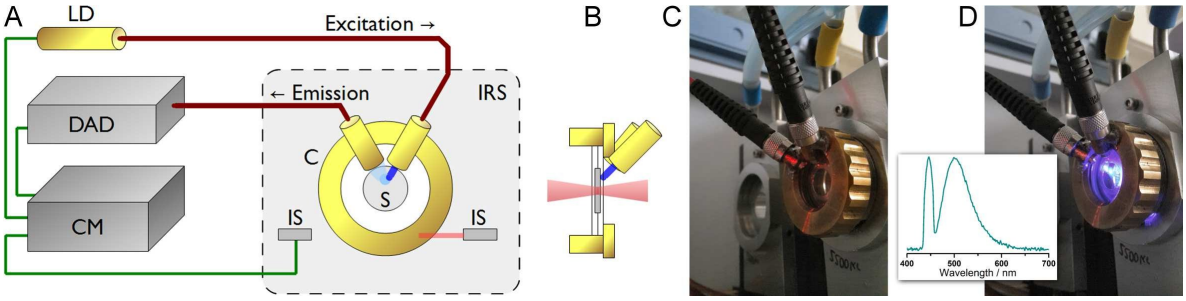

Figure (1) The experimental setup for simultaneous acquisition of infrared, fluorescence and light scattering spectra of proteins. (A) Schematic representation of the setup. Thick, red lines indicate optical fibres, while thin, green lines denote electrical and communication cables. LD: laser diode, DAD: diode-array detector, CM: control module, IS: infrared switch, S: sample, C: purpose-built cell, IRS: infrared spectrometer. The spectrometer sample compartment is indicated by a grey-shaded area around the cell. (B) Cross-section of the infrared cell, showing the orientation of the optical fibres relative to the windows and to the infrared beam (shown in red). (C) and (D) Photographs of the infrared cell and the excitation and probe optical fibres with the 445-nm laser diode switched off and on, respectively. The blue light radiating from the illuminated area corresponds to the back-scattered light and to the fluorescence emission of fibril-bound ThT. The spectrum in (D) is the one recorded by the diode-array detector and shows the sharp, back-scattered laser light (left peak) and the broader fluorescence emission of ThT.

the full range of stages during fibril formation.

Our results show that amyloid fibril formation by βLG is a step-wise process. Destabilisation of the native fold and acid-induced hydrolysis of the polypeptide chain are followed by formation of early aggregates composed of inter-molecular β-sheets. These show an infrared absorption at 1619 cm^{-1}, are large enough to scatter visible light but do not bind ThT, demonstrating their pre-fibrillar nature. Conversion of these pre-fibrillar aggregates into amyloid fibrils leads to an increase in ThT fluorescence after ~5 h, which plateaus after 20–25 h. Further increase in the light scattering signal, together with a moderate, though evident upshift of the 1619-cm^{-1} β-sheet band, indicates that the overall size of the amyloid fibrils is increasing despite the fact that no new fibrils are being formed from monomeric βLG. These changes can be associated to a maturation phase, where individual amyloid fibrils associate to form larger, multi-filament bundles known as *mature* fibrils.

2 Materials and methods

2.1 Materials

HCl (37%) was from VWR (France). ^2H_2O was from Cambridge Isotope Laboratories (Sweden). β-Lactoglobulin from bovine milk (>90% purity) was from Sigma (USA). This sample, containing isoforms A and B, was used without further purification as in several other studies reported in the literature.[55–57]

2.2 Preparation of β-lactoglobulin samples

Lyophilised β-lactoglobulin (βLG) was directly resuspended in 1 mM ThT prepared in ^2H_2O, at a final concentration of 18.4 mg mL^{-1} (1 mM). The sample was mixed carefully until the solution appeared clear by visual inspection. The p^{2}H of the sample was adjusted to a value of 2 (corresponding to a pH-meter reading of 1.6[58]) by μL additions of concentrated ^{2}HCl (100 and 10 mM). The sample was centrifuged for 30 min at 18 000 g and at 4 °C in order to remove undissolved protein or pre-formed aggregates. The supernatant was retrieved and immediately used for the experiments. The protein sample (6 μL) was deposited on a CaF_2 window with a trough of 5 μm. A 100-μm spacer covered with vacuum grease on both sides, was added and the sample was then covered by a flat window. The assembled windows were then mounted in the cell.

2.3 Cell for multispectral analyses

The cell used for the combined acquisition of infrared, fluorescence and light scattering spectra consists of a modified, demountable infrared cell routinely used in our laboratory for analysis of liquid samples. Two hollow rods have been soldered to the screw-in outer ring, allowing for precise and reproducible attachment of two optical fibres (for excitation and emission, respectively) with an inner diameter of 600 μm and fitted with SMA-905 connectors. The fibre ends are oriented with an angle of approximately 45° relative to the CaF_2 window and to each other, and are directed towards a common spot within the sample area. Fluorescence and light scattering are therefore collected at an angle of ∼135°. The distance of the fibre ends from the CaF_2 window is ∼3 mm. Photographs and schemes of the cell are provided in Fig. 1.

2.4 Infrared spectroscopy

Infrared spectra were recorded with a Tensor 37 Fourier-transform spectrometer (Bruker Optics, Germany), equipped with a deuterated tri-glycine sulfate (DTGS) detector and continuously purged with CO_2-free, dry air. The sample cell was mounted on a two-position sample shuttle, which allowed for interleaved acquisition of sample and background spectra. A waiting time of 20 min was allowed after inserting the sample to ensure complete purging. The temperature of the cell was controlled by means of an external water bath circulator. Interferograms were recorded at a resolution of 4 cm^{-1}, apodised using a 3-term Blackman-Harris apodisation function and Fourier-transformed with a zero-filling factor of 4. Sixteen consecutive interferograms were averaged to obtain a single sample or background spectrum. This procedure yields infrared absorption spectra which are virtually devoid of water vapour signals.

Infrared spectra were recorded and analysed using the OPUS software from the instrument manufacturer. Second derivative spectra were calculated using a smoothing length of 13 data points (approx. 13 cm^{-1}). Protein spectra shown throughout the text are uncorrected spectra, *i.e.* the absorption spectrum of ^2H_2O was not subtracted. Infrared spectra

were recorded every 5 min, for 1 h, during heating from 20 to 80 °C, and then every 15 min from 1 to 40 h at 80 °C. The area of the band at 1619 cm^{-1} was integrated between 1624 and 1614 cm^{-1} using the integration option B (straight baseline between the two extremes) in OPUS. Integration was performed on absorption spectra, rather than second derivative spectra, since band shifts and line width changes has a lesser effect in the former.

2.5 Fluorescence and light scattering measurements

The light source consists of a 445±5 nm laser diode (Thorlabs, Sweden), with a nominal output power of 4.5 mW. The fluorescence emission of ThT and the back-scattered light were recorded simultaneously using an AvaSpec-1024 diode-array detector (Avantes, Netherlands) receiving light from the sample in the infrared spectrometer via the probe optical fibre. A plastic filter with a high 482 nm to 445 nm transmittance ratio (T_{482}/T_{445} = 3.23) was placed between the probe optical fibre and the detector to attenuate the intense back-scattered light (the transmission spectrum of the filter is shown in Fig. 3, panel B). This allowed recording of both signals in the same spectrum without saturation of either and eliminated the need to record two distinct spectra with different integration times. The integration time used to record the spectra shown in this study is 3 s. Spectra were recorded using the AvaSpec software from the detector manufacturer and analysed using OPUS. The back-scattering band (445 nm) and the ThT emission band (500 nm) were integrated between 435 and 445 nm, and between 470 and 530 nm, respectively, using the integration option B (straight baseline between the two extremes) in OPUS.

Acquisition of fluorescence and light scattering spectra in our system is triggered by movement of the sample stage onto the sample position. This is preceded by activation of the laser diode, which is allowed to stabilise for 5 seconds. A first spectrum ("lit" spectrum) is recorded and stored. The laser diode is then switched off and a second spectrum ("dark" spectrum) is recorded and stored. This allows the removal of the intrinsic, light-independent signal of each pixel and to obtain spectra with a flat baseline. The total illumination time for each spectrum is 15 s.

2.6 Transmission electron microscopy

For transmission electron microscopy (TEM) analyses, fibrillated βLG samples were diluted with ddH_2O to a final protein concentration of 1 mg mL^{-1} and 10 μL were deposited on a parafilm sheet. A carbon- and formvar-coated, 200-mesh copper grid (Ted Pella, USA) was placed face-down onto the sample droplet and let to sit for 5 min. This procedure minimises adhesion of large particles to the grid. Excess sample was removed by careful blotting with the side of a laboratory paper wipe and the grid was immediately stained by placing it onto a 10 μL drop of 2% uranyl acetate. Excess stain was removed by blotting, and the grid was let air dried. TEM images were acquired with a TECNAI G2 Spirit Bio TWIN (FEI, USA) at an operating voltage of 80 kV.

3 Results

3.1 The integrated system for multispectral analysis

Our experimental setup for multispectral analysis is shown in Fig. 1 and consists of the following parts: (1) a light source (LD) that illuminates the sample, exciting the fluorophore (ThT) and providing monochromatic radiation for the light scattering measurement; (2) a diode-array detector (DAD) that records light over the entire visible range, allowing for simultaneous measurement of the fluorophore emission and the light scattered by the sample; (3) a modified infrared cell (C) where two optical fibres, one connected to the light source and the other to the diode-array detector, can be reproducibly focussed on the same spot of the sample; (4) a custom-built, electronic control module (CM) that connects to the infrared spectrometer and synchronises acquisition of infrared spectra with triggering of the light source and of the diode-array detector; (5) a commercial infrared spectrometer (IRS) equipped with a sample-shuttling stage.

The light source used for light scattering and ThT excitation is a commercial laser diode with an emission maximum at ∼445 nm. The control module is based on an Arduino MICRO prototyping board (Arduino, Italy). It is connected to a contactless infrared switch inside the sample compartment, which closes when the shuttling stage moves into position to record the sample infrared spectrum. This signal switches the laser diode on via the control module. After a delay to allow the laser diode to stabilise, the diode-array detector is triggered to record and save the "lit" (laser diode on) and "dark" (laser diode off) spectra.

3.2 Infrared absorption of native and denatured βLG

The second derivative spectrum of βLG at 20 °C, p^{2}H 2, is shown in Fig. 2 (blue trace). Five well-resolved component bands can be observed in the amide I' region (1700–1610 cm^{-1}). The sharp bands at 1632 cm^{-1} (intense) and the 1692 cm^{-1} (weak) can be assigned to the low- and high-frequency components of antiparallel β-sheets, while the band at 1651 cm^{-1} can be assigned to α-helices.[39,40,59,60] These observations are in agreement with previous infrared studies of βLG available in the literature[61,62] and suggest that under the conditions used the protein adopts its native structure consisting of an antiparallel β-barrel core flanked by an α-helix.[63]

The weaker bands at 1680 and 1665 cm^{-1} can be assigned to turns. Bands outside the amide I' range can be assigned to amino acid side chains. These include the broad absorption near 1715 cm^{-1} originating from the protonated carboxylic groups of Asp and Glu residues, and the band at 1515 cm^{-1}, arising from tyrosine residues, respectively.[64] The weak absorption at approx. 1550 cm^{-1} originates from the residual amide II band, *i.e.* N—H groups in stable peptide bonds which have not undergone H/^{2}H exchange.[40]

Increasing the temperature to 80 °C leads to dramatic changes in the amide I' band. The strong low-frequency band of antiparallel β-sheets has decreased to approx. one third of its initial intensity, while the high-frequency component has disappeared or, more probably, it has shifted to lower (∼1680 cm^{-1}) wavenumbers. In a similar way, the sharp α-helix band

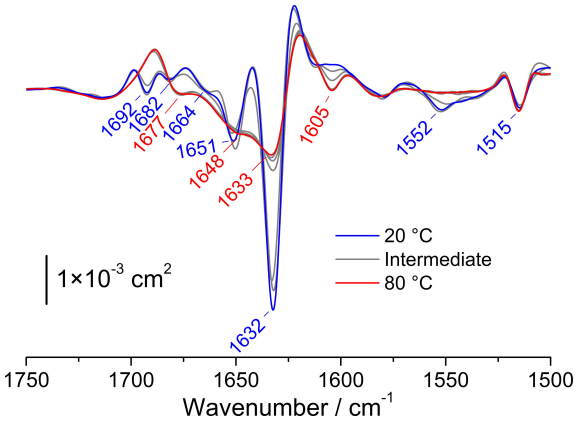

Figure (2) Second derivative spectra of βLG recorded during heating from 20 to 80 °C. The spectrum recorded at 20 °C is shown in blue, the one at 80 °C is shown in red. Spectra at intermediate temperatures are shown in grey. The origin of the labelled bands is described in the text.

has disappeared. These changes are accompanied by the appearance of a broad band at $\sim$1645 cm^{-1}, which can be ascribed to random coil conformations. Altogether, the spectral changes described so far suggest that the native structure has been significantly destabilised. This is corroborated by the loss of the residual amide II band, indicating that the peptide bonds previously involved in stable secondary structures are now exposed to the deuterated solvent.

Interestingly, structure loss leads to a clear band at 1605 cm^{-1} which can be assigned to arginine. A possible explanation is that several arginine residues became hydrogen-bonded to solvent molecules, rather than being involved in specific interactions with other protein residues. This makes arginine absorption more homogeneous in the denatured state, whereas it is more outspread over a large spectral range in the native conformation. No sign of aggregation can be observed in the spectra after 1 h at 80 °C (Fig. 2, red trace), because of the absence of a band between 1620 and 1610 cm^{-1} arising from inter-molecular β-sheets.

3.3 Infrared, fluorescence and light scattering measurements of βLG under amyloid-forming conditions

The infrared absorption of βLG incubated at 80 °C, p^{2}H 2, at several time points (5, 10, 20, 30 and 40 h) is shown in Fig. 3, panel A. The most noticeable feature for the spectrum after 5 h incubation (Fig. 3, blue trace) as compared to the spectrum after 1 h (Fig. 2, red trace) is further loss of the native antiparallel β-sheet band. Instead, a band now becomes visible at higher wavenumber (1638 cm^{-1}). This band has been probably present before but hidden under the larger 1632 cm^{-1} band as we do not find evidence for its formation in our spectra. The band position at 1638 cm^{-1} suggests that the corresponding β-sheet is composed of fewer strands or is more distorted than the β-sheet that dominates the native structure.[38] Both properties decrease the strength of vibrational coupling between C=O oscillators within the sheet and shift their absorptions to higher wavenumbers.

At the same time a sharp band appears at approx. 1619 cm^{-1}, indicating formation of inter-molecular β-sheets.[65] The band continues to grow throughout the experiment and experiences a small upshift with time as shown in the inset of Fig. 3A.The absence of a high-frequency component (usually between 1685 and 1680 cm^{-1} in ^2H_2O) suggests that the β-sheets have a parallel arrangement. Loss of the solvated arginine signal at 1605 cm^{-1} seems to occur simultaneously with protein aggregation, thereby strengthening the hypothesis that this side chain may be involved in specific interactions in structured forms (native or fibrillated) of βLG. In line with this, the Arg band seems to shift to lower wavenumbers, where a new band forms at 1596 cm^{-1}.

Panel B shows the back-scattering and fluorescence emission spectra recorded by our system at the same time points as the infrared spectra in panel A. Two signals can be observed in these spectra: a sharp signal at 445 nm originating from the visible light that is back-scattered by the sample, and a broad signal at 500 nm, originating from the fluorescence emission of fibril-bound ThT. The difference between the position of the ThT emission maximum in our spectra and the one commonly observed for fibril-found ThT (482 nm) originates from the optical filter used to decrease the scatter/fluorescence ratio. The real spectrum "emitted" by the sample can easily be obtained by ratioing the recorded spectrum by the transmission spectrum of the filter (shown as a dashed line). This procedure is neither required for quantitative measurements, nor for kinetic analyses and so has been omitted.

The intensities of the back-scattered light and the fluorescence of ThT increase during incubation of βLG under amyloid-forming conditions. This indicates that large particles are forming in the temporal window under investigation, and that they consist of amyloid fibrils.

3.4 Kinetics of fibril formation: evidence for aggregation intermediates

The results presented above prove that the proposed experimental setup allows for simultaneous acquisition of infrared, light scattering and fluorescence spectra of proteins during aggregation and that it can help elucidate important processes in fibril formation. For instance, it is possible to determine whether an aggregate is amorphous (no ThT fluorescence) or fibrillar (ThT fluorescence).

More insightful information can be obtained by comparing time-dependent changes in back-scattering intensity and ThT fluorescence to those of specific, structure-reporting bands in the infrared spectrum of a protein undergoing aggregation. To demonstrate this, the aggregation band at 1619 cm^{-1}, the fluorescence emission band of ThT at 500 nm and the back-scattered band at 445 nm were integrated and their band areas were plotted as a function of the incubation time. The results can be observed in Fig. 3, panels C–E. The three plots show different profiles. The aggregation band at 1619 cm^{-1} shows an apparent exponential behaviour, while the ThT emission shows a sigmoidal trend with a lag phase between 0 and 5 h. The back-scattering signal shows a more complex bi-phasic profile, which appears to be the sum of two distinct processes occurring at different times during the aggregation process. Although the three curves might look remarkably different from one another, they

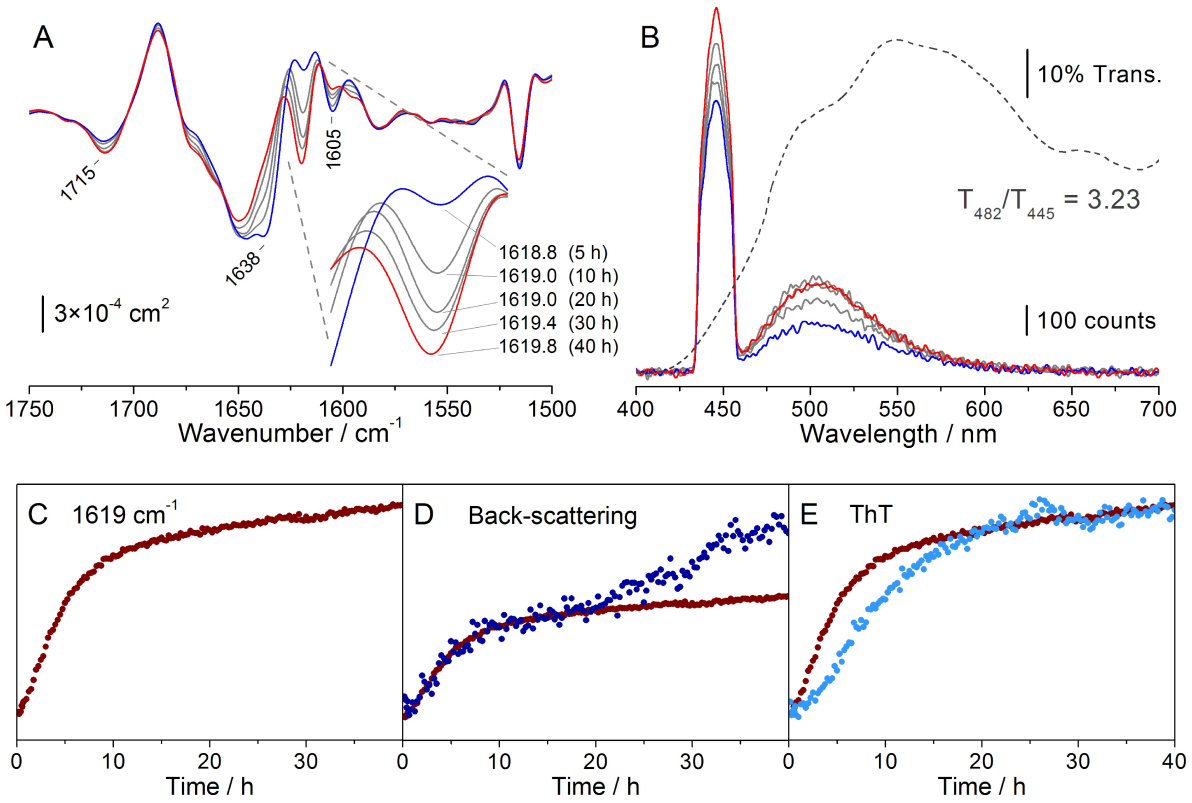

Figure (3) Infrared, fluorescence and light scattering spectra of βLG under amyloid-forming conditions. (A) Second derivative infrared spectra of βLG at different time points (5, 10, 20, 30, 40 h). The inset shows shows the changes in intensity and position of the aggregation band at ~1619 cm^{-1}. (B) ThT emission and light scattering spectra recorded at the same time-points as in (A). The transmission spectrum of the filter used to attenuate the back-scattered light is overlayed to the spectra and shown as a dashed line. (C–E) Time-dependent changes in the areas of the band at 1619 cm^{-1}, of the back-scattered band at 445 nm and of the ThT emission band at 500 nm, respectively. The integration ranges are described in Materials and Methods. The trace of the 1619-cm^{-1} fibril band shown in (A) is superimposed to those in (D) and (E), after normalization between 0 and 20 h.

all seem to plateau after approx. 20–25 h, with the exception of the second phase in the back-scattering plot. Comparison of the three curves normalised to the same intensity at 20 h reveals, for instance, that the aggregation band at 1619 cm^{-1} and the first phase of the back-scattering signal at 445 nm show the same time profile (Fig. 3, panel D), indicating that they are related to the same phenomenon.

Unlike back-scattering, superimposition of the ThT trace with that of the 1619-cm^{-1} band reveals that they originate from two different phenomena. The observation that the early-phase aggregation of βLG is not accompanied by proportional binding of ThT suggests the existence of transient aggregates with a dominant β-sheet architecture, but with structural and/morphological properties different to those of amyloid fibrils. The identity of these species fully coincides with oligomeric and/or pre-fibrillar species described in a recent study by Torreggiani and co-workers,[55] as well as in other previous studies.[66,67]

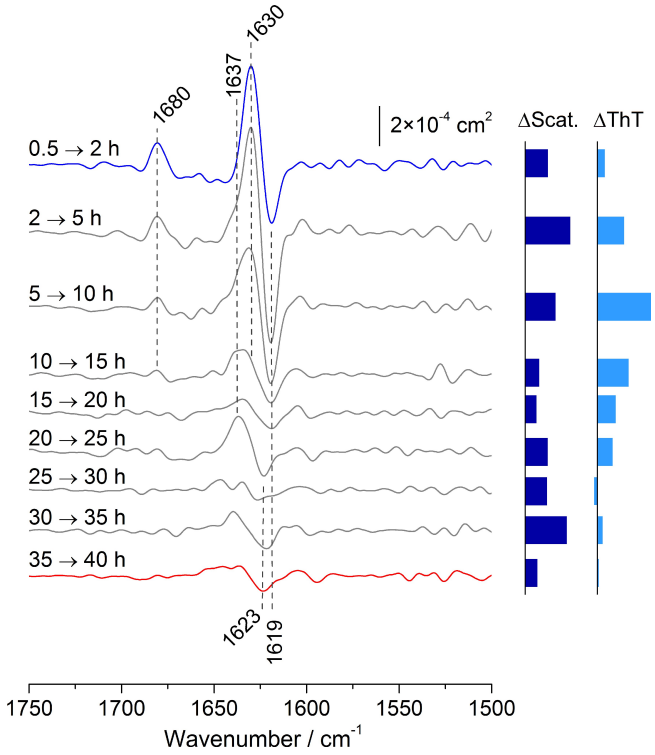

Figure (4) Difference spectra of the second derivatives recorded during fibril formation. Difference spectra were calculated by subtracting the second derivative spectrum recorded at give time point (T_1), from that of one recorded at a later time point (T_2). Negative bands correspond to intensity increases in the original absorption spectra over time.

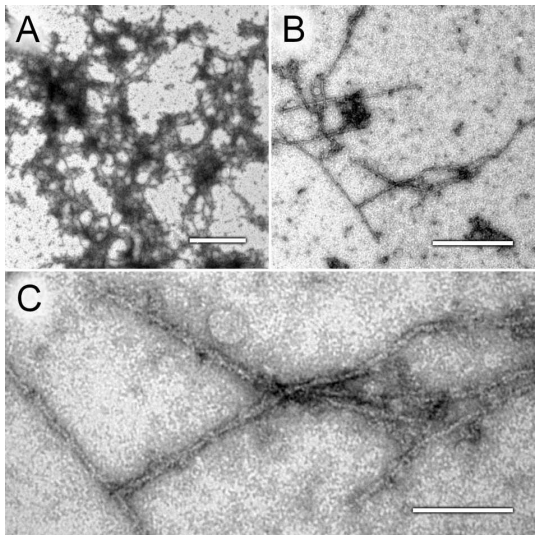

Figure (5) TEM images of βLG fibrils. TEM images of βLG fibrils after incubation at 80 °C (p^{2}H 2) for 40 h. The samples were stained with 2% uranyl acetate as described in Materials and Methods. Scale bars in panels A–C correspond to 1 μm, 300 nm and 100 nm, respectively.

The analysis of the kinetic data from the three spectroscopic methods has revealed three processes:
(i) Formation of β-sheet containing pre-fibrillar aggregates. They are characterised by increased light scattering, formation of the 1619 cm^{-1} band and a lack of ThT fluorescence.
(ii) Formation of amyloid fibrils characterised by an enhanced ThT fluorescence.
(iii) Formation of larger fibrils as demonstrated by the increase in light scattering.

We were then interested whether these processes reflect in the infrared spectra. To this end, we calculated the difference between second derivative spectra taken at different times. These are shown in Fig. 4. In these difference spectra, strong positive bands indicate structures that disappear with time, whereas strong negative bands indicate structures that form. Within the first 10 h, the difference spectra are similar regarding their main features and indicate the disappearance of structures with absorption near 1680 and 1630 cm^{-1} from the partly denatured native structure as well as the formation of structures absorbing at 1619 cm^{-1}. The disappearing high frequency band indicates that this transition involves the transformation of antiparallel β-sheets to parallel β-sheets.

It was already noted that a band at 1638 cm^{-1} becomes visible early in the aggregation process and disappears later. The disappearance of the 1638-cm^{-1} band in the second derivative spectra (Fig. 3A) gives rise to the broadening on the high wavenumber side of the main positive band seen in the second and third difference spectrum. From the 4th difference spectrum on (10 $\rightarrow$ 15h), the 1638-cm^{-1} band becomes more prominent and is observed throughout the aggregation process.

The first 15 h of aggregation cover the lag phase and the exponential phase of ThT fluorescence. In particular, the first difference spectrum is calculated where the ThT fluorescence is low but the 1619-cm^{-1} absorption increases exponentially. Thus it should be dominated by formation of pre-fibrillarrillar aggregates. At later times, the ThT fluorescence increases strongly. Nevertheless the difference spectra are very similar to the first difference spectrum. In particular the band position at 1619 cm^{-1} of the forming species does not change. This indicates that the architecture of pre-fibrillar aggregates and of the initial fibrils is similar from the infrared perspective which extends over a range of 10–15 strands in a β-sheet. Both aggregates seem to consist of parallel β-sheets.

The late difference spectra cover the second phase in the light scattering profile which does not seem to correlate with either the fluorescence emission of ThT or with changes in the intensity of the aggregation band at 1619 cm^{-1}. This phase begins at approx. 25 h, where the other two plots have nearly plateaued. This suggests that although no new fibrils are being formed from soluble βLG, the overall size of the particles is increasing. This scenario is consistent with a maturation phase of the single amyloid fibrils, which associate to form thicker fibres. Macroscopic phenomena like this one cannot easily be studied by infrared spectroscopy in the mid-IR range. Nevertheless, the second-derivative spectra, some of which are shown in Fig. 3 A, show that the aggregation band slowly shifts to higher wavenumbers after 20h. The shift is particularly clear in the difference spectra shown in Fig. 4, where a negative band at $\sim$1623 cm^{-1} can be observed in the 20 $\rightarrow$ 25 h difference

spectrum. This indicates that the β-sheet band of the fibrils formed in the second phase is upshifted compared to those formed initially. Recent theoretical work by Karjalainen and Barth[68] has shown that stacking of β-sheets, such as in mature amyloid fibrils, induces an upshift of the main β-sheet band. The magnitude of the shift is highest (5 cm^{-1}) when the intersheet distance between two stacked sheets is 5 Å and the orientation is 0° or 180°. Therefore, the second phase in the light scattering profile might very well arise from association of individual fibrils into higher-order structures. This property of βLG fibrils has, indeed, been observed in a time-dependent DLS study.[55] In an AFM study, Mezzenga and co-workers have directly observed the co-existence of βLG fibrils comprising 1–5 filaments and thus suggested a "hierarchical multi-stranded self-assembly scheme".[57] The same phenomenon has been observed by small angle neutron scattering.[69]

TEM images of βLG fibrils at the end of the incubation period (Fig. 5) show the presence of unbranched fibrils with a length of several hundred nm and a thickness of approx. 8–12 nm. Direct comparison between TEM and AFM images may be problematic since these techniques require distinct procedures for sample preparation. In addition, it is the stain, not the sample, that is directly observed in electron microscopy. With these limitations in mind, the diameter of the βLG fibrils in our preparations seems to be compatible with bundles comprising 3–5 filaments shown in the AFM study described above, rather than with single fibrils ($\sim$2 nm in diameter). Another possible explanation for the upshift of the fibril band is an increase in the twist of the fibril (*i.e.* fewer strands per turn). Mezzenga and co-workers, however, have observed a decrease of the twist upon later association of βLG fibrils, leading to a regular increase in the period from 36 nm for fibrils comprising two strands, to 144 nm for fibrils comprising five strands.

3.5 Effect of cooling on the infrared, fluorescence and light scattering spectra of βLG fibrils

Fig. 6 shows the infrared (panel A) and light scattering/fluorescence spectra (panel B) of the aggregated βLG sample during cooling from 80 °C (red trace) to 20 °C (blue trace) within $\sim$1.5 h. This allows to study the effect of temperature on the fibril structure, as well as on the non-aggregated protein. Cooling has a negligible effect on the fibril band, the intensity of which remains unaltered. This suggests that the fibrils formed under our experimental conditions consist of stable structures. The downshift of the band position from 1620 to 1618 cm^{-1} suggests decreased conformational flexibility of the fibrils, for it denotes stronger vibrational coupling among C=O oscillators within the β-sheets. Cooling also induces a significant decrease of the random coil band at 1648 cm^{-1}, with a concomitant increase of a band at 1638 cm^{-1}. The origin of this band cannot be univocally identified, but it might arise from β-sheets with a limited number of strands ($\sim$2–4). Vibrational coupling is weaker in these structures than in larger sheets (compare, for instance, the position of the β-sheet band in native βLG shown in Fig. 2) and therefore the band appears to be at higher wavenumbers. This is in agreement with several other studies, which have demonstrated that the amyloidogenic component in βLG does not coincide with the entire protein, but rather with unstructured,

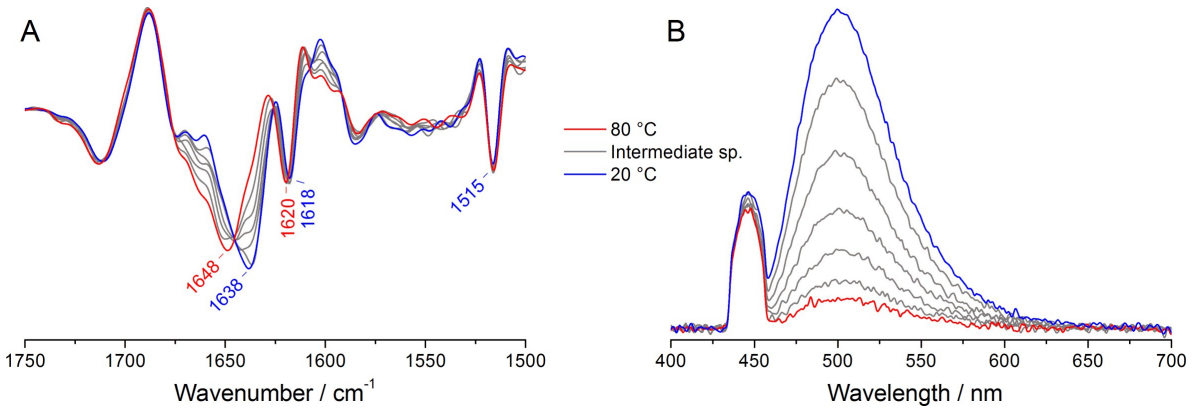

Figure (6) Infrared, fluorescence and light scattering spectra of βLG during cooling from 80 °C to 20 °C. (A) Second derivative spectra. (B) light scattering and ThT emission. The spectrum recorded at 80 °C is shown in red, the one at 20 °C is shown in blue. Spectra at intermediate temperatures are shown in grey. The origin of the labelled bands is described in the text.

hydrolytic fragments (between 2 and 8 kDa) detached from the protein following incubation at low pH and high temperatures.[56,70] It is therefore plausible that, at low temperatures, the fragments still in solution might refold into stretches of the original β-sheet. This observation is corroborated by the fact that the the intensity of the scattered light remains unaltered (Fig. 6, panel B), and therefore no large aggregates are formed. The weak increase in the back-scattering intensity is due to overlap with the low-wavelength side of the ThT emission. A ten-fold increase in ThT emission of ThT can be observed. This stems, at least in part, from the increase in quantum yield brought about by the lower temperature.[71,72] A further possible explanation for the increased fluorescence after cooling could be a higher affinity of the dye for the fibrils at lower temperatures.

4 Discussion

Amyloid fibril formation is a fascinating, yet poorly understood phenomenon with several implications in human health. The number of stages and species involved poses a challenge to a comprehensive understanding of this process. This must, therefore, be addressed using several experimental approaches simultaneously. To this purpose, we have designed and built a combined system for simultaneous infrared, fluorescence and light scattering measurements of proteins during amyloid fibril formation or, more in general, during aggregation. Each of these spectroscopic techniques allows the examination of a specific aspect of amyloid fibrils and pre-fibrillar species. Infrared spectroscopy provides structural details as it studies the formation/loss of and conformational changes in secondary structure. Its sensitivity towards β-sheets makes it particularly valuable in the study of amyloid. Fluorescence emission of the amyloid-specific dye ThT allows to distinguish between fibrillar and amorphous aggregates. It also enables the monitoring of the kinetics of fibril formation, and therefore the study of the underlying polymerisation mechanism. Light scattering allows to

monitor changes in the overall size of the aggregates. It is particularly useful in the study of processes that lead to increases in particle size without changes in protein structure or tinctorial properties, such as bundling of single amyloid fibrils into mature fibrils.

These three spectroscopic techniques have never before been combined into a single, multispectral analysis. Compared to performing three separate analyses with three different samples, or with the same sample "shuttled" continuously among several instruments, our approach allows the elucidation of the intimate connection between structure, microscopic and macroscopic properties of amyloid fibrils.

The setup presented in this paper is cost-effective and versatile. It can easily be installed onto commercial infrared spectrometers. At a cost of ∼200 USD (180 EUR), the 445-nm laser diode used for ThT excitation and light scattering in our study is relatively cheap, but already more expensive than most laser diode modules of more common wavelengths. This means that virtually any other fluorophore can be included in the analysis at a very moderate cost. In addition to this, the use of a bifurcated fibre optic cable and two different light sources would allow to study two fluorophores simultaneously. An additional fluorophore could be one that is sensitive to the denaturation state of the protein by binding to exposed hydrophobic regions, such as 8-anilino-1-naphthalenesulfonic acid (λ_{ex} = 380 nm, λ_{em} = 470 nm) or Sypro Orange (λ_{ex} = 472 nm, λ_{em} = 570 nm). FRET studies conducted using pairs of donor and acceptor fluorophores (*e.g.* fluorescein and rhodamine) are another useful implementation.

When tested on β-lactoglobulin (βLG), a model protein in the study of amyloid fibrils and a major whey protein of interest to the food industry, our approach successfully allowed the study of all the processes occurring during fibril formation by this protein, from destabilisation of the soluble, monomeric protein, to formation of early, non-fibrillar aggregates, to formation of amyloid fibrils and, at a later stage, further maturation of the individual fibrils into mature, multi-filament fibrils. In particular, the following phases were observed with our approach:

(i) During the initial phase of aggregation, light scattering increases and residual native, antiparallel β-sheet structure (infrared bands at 1680 and 1630 cm^{-1}) is lost while extended, flat parallel β-sheets (1619-cm^{-1} infrared band) are formed. They are characteristic for the pre-fibrillar aggregates, since they are formed already in the lag phase of ThT fluorescence.

(ii) These processes continue during fibril formation as defined by an increase in the ThT fluorescence. Since there is no detectable change between the infrared spectrum of the aggregates formed during the lag and the exponential phases of ThT fluorescence, the β-sheet architecture of the pre-fibrillar aggregates and of the fibrils seem to be similar on the length scale of infrared spectroscopy, *i.e.* several strands. At the same time, a further β-sheet species (1638 cm^{-1} infrared band), which contains fewer strands or is more distorted than the β-sheet of the native structure, starts to decay and is likely incorporated into the same 1619-cm^{-1} β-sheet structures.

(iii) Maturation of the fibrils makes them larger as indicated by an increase in light scattering. At the same time the main infrared band shifts upwards which indicates a structural

change on the length scale detected by infrared spectroscopy. The shift is consistent with the formation of β-sheet layers which occurs when fibrils associate to fibril bundles.

In conclusion, the multispectral approach and the custom-built setup illustrated in this paper can provide insightful details on amyloid fibril formation, and can easily be adapted to study other processes in proteins.

5 Acknowledgments

This work was supported by a grant from Alzheimerfonden (to A.B.) and a post-doctoral fellowship from Wenner-Gren Stiftelsen (to M.B.). Knut och Alice Wallenbergs Stiftelsen and Lars Hiertas Minne Stiftelsen are gratefully acknowledged for providing the spectrometer and the sample shuttle, respectively. Anna-Stina Höglund is acknowledged for assistance with TEM imaging. The authors thank Torbjörn Astlind for machining of the modified infrared cuvette used in this study.

References

[1] Ami, D., Natalello, A., Lotti, M., and Doglia, S. M. *Microb Cell Fact* **12**, 17 (2013).
[2] Lapidus, L. J. *Mol Biosyst* **9**(1), 29–35 Jan (2013).
[3] Ross, C. A. and Poirier, M. A. *Nat Rev Mol Cell Biol* **6**(11), 891–8 Nov (2005).
[4] Aguzzi, A. and O'Connor, T. *Nat Rev Drug Discov* **9**(3), 237–48 Mar (2010).
[5] Singh, T. K., Øiseth, S. K., Lundin, L., and Day, L. *Food Funct* **5**(11), 2686–98 Nov (2014).
[6] Delahaije, R. J. B. M., Wierenga, P. A., Giuseppin, M. L. F., and Gruppen, H. *J Agric Food Chem* **63**(21), 5257–65 Jun (2015).
[7] Costantino, H. R., Langer, R., and Klibanov, A. M. *Pharm Res* **11**(1), 21–9 Jan (1994).
[8] den Engelsman, J., Garidel, P., Smulders, R., Koll, H., Smith, B., Bassarab, S., Seidl, A., Hainzl, O., and Jiskoot, W. *Pharm Res* **28**(4), 920–33 Apr (2011).
[9] Philo, J. S. and Arakawa, T. *Curr Pharm Biotechnol* **10**(4), 348–51 Jun (2009).
[10] Morris, A. M., Watzky, M. A., and Finke, R. G. *Biochim Biophys Acta* **1794**(3), 375–97 Mar (2009).
[11] Invernizzi, G., Papaleo, E., Sabate, R., and Ventura, S. *Int J Biochem Cell Biol* **44**(9), 1541–54 Sep (2012).
[12] Pauling, L. and Itano, H. A. *Science* **109**(2835), 443 Apr (1949).
[13] Gravitz, L. and Pincock, S. *Nature* **515**(7526), S1 Nov (2014).
[14] Chiti, F. and Dobson, C. M. *Annu Rev Biochem* **75**, 333–66 (2006).
[15] Harrison, R. S., Sharpe, P. C., Singh, Y., and Fairlie, D. P. *Rev Physiol Biochem Pharmacol* **159**, 1–77 (2007).
[16] Knowles, T. P. J., Vendruscolo, M., and Dobson, C. M. *Nat Rev Mol Cell Biol* **15**(6), 384–96 Jun (2014).

[17] Serpell, L. C., Sunde, M., Benson, M. D., Tennent, G. A., Pepys, M. B., and Fraser, P. E. *J Mol Biol* **300**(5), 1033–9 Jul (2000).

[18] Serpell, L. C. *Biochim Biophys Acta* **1502**(1), 16–30 Jul (2000).

[19] Nelson, R., Sawaya, M. R., Balbirnie, M., Madsen, A. Ø., Riekel, C., Grothe, R., and Eisenberg, D. *Nature* **435**(7043), 773–8 Jun (2005).

[20] Jahn, T. R., Makin, O. S., Morris, K. L., Marshall, K. E., Tian, P., Sikorski, P., and Serpell, L. C. *J Mol Biol* **395**(4), 717–27 Jan (2010).

[21] El-Agnaf, O. M. A., Walsh, D. M., and Allsop, D. *Lancet Neurol* **2**(8), 461–2 Aug (2003).

[22] Haass, C. and Selkoe, D. J. *Nat Rev Mol Cell Biol* **8**(2), 101–12 Feb (2007).

[23] Citron, M. *Nat Rev Drug Discov* **9**(5), 387–98 May (2010).

[24] Beitz, J. M. *Front Biosci (Schol Ed)* **6**, 65–74 (2014).

[25] Bates, G. P., Dorsey, R., Gusella, J. F., Hayden, M. R., Kay, C., Leavitt, B. R., Nance, M., Ross, C. A., Scahill, R. I., Wetzel, R., Wild, E. J., and Tabrizi, S. J. *Nature Reviews Disease Primers* , 15005 EP – 04 (2015).

[26] Westermark, P., Andersson, A., and Westermark, G. T. *Physiol Rev* **91**(3), 795–826 Jul (2011).

[27] Lusis, A. J. *Nature* **407**(6801), 233–41 Sep (2000).

[28] Robberecht, W. and Philips, T. *Nat Rev Neurosci* **14**(4), 248–64 Apr (2013).

[29] Zandomeneghi, G., Krebs, M. R. H., McCammon, M. G., and Fändrich, M. *Protein Sci* **13**(12), 3314–21 Dec (2004).

[30] Scirè, A., Baldassarre, M., Galeazzi, R., and Tanfani, F. *Biochimie* **95**(2), 158–66 Feb (2013).

[31] Sarroukh, R., Goormaghtigh, E., Ruysschaert, J.-M., and Raussens, V. *Biochim Biophys Acta* **1828**(10), 2328–38 Oct (2013).

[32] Buchanan, L. E., Carr, J. K., Fluitt, A. M., Hoganson, A. J., Moran, S. D., de Pablo, J. J., Skinner, J. L., and Zanni, M. T. *Proc Natl Acad Sci U S A* **111**(16), 5796–801 Apr (2014).

[33] Hernik, A., Pulawski, W., Fedorczyk, B., Tymecka, D., Misicka, A., Filipek, S. H., and Dzwolak, W. *Langmuir* Sep (2015).

[34] Miller, L. M., Bourassa, M. W., and Smith, R. J. *Biochim Biophys Acta* **1828**(10), 2339–46 Oct (2013).

[35] Shivu, B., Seshadri, S., Li, J., Oberg, K. A., Uversky, V. N., and Fink, A. L. *Biochemistry* **52**(31), 5176–83 Aug (2013).

[36] Lotti, S. M. D. M., editor. *rotein Aggregation in Bacteria: Functional and Structural Properties of Inclusion Bodies in Bacterial Cells*. Protein and Peptide Science. Wiley, (2014).

[37] Yang, H., Yang, S., Kong, J., Dong, A., and Yu, S. *Nat Protoc* **10**(3), 382–96 Mar (2015).

[38] Barth, A. and Zscherp, C. *Q Rev Biophys* **35**(4), 369–430 Nov (2002).

[39] Kong, J. and Yu, S. *Acta Biochim Biophys Sin (Shanghai)* **39**(8), 549–559 Aug (2007).

[40] Barth, A. *Biochim Biophys Acta* **1767**(9), 1073–1101 Sep (2007).

[41] Boulet-Audet, M., Lefèvre, T., Buffeteau, T., and Pézolet, M. *Appl Spectrosc* **62**(9), 956–62 Sep (2008).

[42] Sarroukh, R., Cerf, E., Derclaye, S., Dufrêne, Y. F., Goormaghtigh, E., Ruysschaert, J.-M.,

and Raussens, V. *Cell Mol Life Sci* **68**(8), 1429–38 Apr (2011).
[43] Cerf, E., Sarroukh, R., Tamamizu-Kato, S., Breydo, L., Derclaye, S., Dufrêne, Y. F., Narayanaswami, V., Goormaghtigh, E., Ruysschaert, J.-M., and Raussens, V. *Biochem J* **421**(3), 415–23 Aug (2009).
[44] Khurana, R., Coleman, C., Ionescu-Zanetti, C., Carter, S. A., Krishna, V., Grover, R. K., Roy, R., and Singh, S. *J Struct Biol* **151**(3), 229–38 Sep (2005).
[45] Biancalana, M. and Koide, S. *Biochim Biophys Acta* **1804**(7), 1405–12 Jul (2010).
[46] LeVine, 3rd, H. *Methods Enzymol* **309**, 274–84 (1999).
[47] Meisl, G., Yang, X., Hellstrand, E., Frohm, B., Kirkegaard, J. B., Cohen, S. I. A., Dobson, C. M., Linse, S., and Knowles, T. P. J. *Proc Natl Acad Sci U S A* **111**(26), 9384–9 Jul (2014).
[48] Wyatt, P. J. *Analytica Chimica Acta* **272**(1), 1–40 (1993).
[49] Georg, H., Barth, A., Kreutz, W., Siebert, F., and Mäntele, W. *Biochim Biophys Acta* **1188**(1-2), 139–50 Nov (1994).
[50] Li, Y., Maurer, J., Roth, A., Vogel, V., Winter, E., and Mäntele, W. *Rev Sci Instrum* **85**(8), 084302 Aug (2014).
[51] Hoffmann, M. A. and van Mil, P. J. *J Agric Food Chem* **47**(5), 1898–905 May (1999).
[52] Yan, Y., Seeman, D., Zheng, B., Kizilay, E., Xu, Y., and Dubin, P. L. *Langmuir* **29**(14), 4584–93 Apr (2013).
[53] Leeb, E., Götz, A., Letzel, T., Cheison, S. C., and Kulozik, U. *Food Chem* **187**, 545–54 Nov (2015).
[54] Oboroceanu, D., Wang, L., Brodkorb, A., Magner, E., and Auty, M. A. E. *J Agric Food Chem* **58**(6), 3667–73 Mar (2010).
[55] Navarra, G., Tinti, A., Di Foggia, M., Leone, M., Militello, V., and Torreggiani, A. *J Inorg Biochem* **137**, 64–73 Aug (2014).
[56] Akkermans, C., Venema, P., van der Goot, A. J., Gruppen, H., Bakx, E. J., Boom, R. M., and van der Linden, E. *Biomacromolecules* **9**(5), 1474–9 May (2008).
[57] Adamcik, J., Jung, J.-M., Flakowski, J., De Los Rios, P., Dietler, G., and Mezzenga, R. *Nat Nanotechnol* **5**(6), 423–8 Jun (2010).
[58] Lumry, R., Smith, E. L., and Glantz, R. R. *Journal of the American Chemical Society* **73**(9), 4330–4340 (1951).
[59] Surewicz, W. K., Mantsch, H. H., and Chapman, D. *Biochemistry* **32**(2), 389–394 Jan (1993).
[60] Paquet-Mercier, F., Lefevre, T., Auger, M., and Pezolet, M. *Soft Matter* **9**, 208–215 (2013).
[61] Casal, H. L., Köhler, U., and Mantsch, H. H. *Biochim Biophys Acta* **957**(1), 11–20 Nov (1988).
[62] Ioannou, J., Donald, A., and Tromp, R. *Food Hydrocolloids* **46**, 216 – 225 (2015).
[63] Kontopidis, G., Holt, C., and Sawyer, L. *J Dairy Sci* **87**(4), 785–96 Apr (2004).
[64] Barth, A. *Prog Biophys Mol Biol* **74**(3-5), 141–173 (2000).
[65] Dong, A., Randolph, T. W., and Carpenter, J. F. *J Biol Chem* **275**(36), 27689–93 Sep (2000).
[66] Bauer, R., Carrotta, R., Rischel, C., and Øgendal, L. *Biophysical Journal* **79**, 1030–1038

(2000).

[67] Carrotta, R., Bauer, R., Waninge, R., and Rischel, C. *Protein Sci* **10**(7), 1312–8 Jul (2001).

[68] Karjalainen, E.-L., Ravi, H. K., and Barth, A. *J Phys Chem B* **115**(4), 749–57 Feb (2011).

[69] Bolisetty, S., Adamcika, J., and Mezzenga, R. *Soft Matter* **7**, 493–499 (2011).

[70] Dave, A. C., Loveday, S. M., Anema, S. G., Loo, T. S., Norris, G. E., Jameson, G. B., and Singh, H. *J Agric Food Chem* **61**(32), 7817–28 Aug (2013).

[71] Stsiapura, V. I., Maskevich, A. A., Kuzmitsky, V. A., Uversky, V. N., Kuznetsova, I. M., and Turoverov, K. K. *J Phys Chem B* **112**(49), 15893–902 Dec (2008).

[72] Sulatskaya, A. I., Maskevich, A. A., Kuznetsova, I. M., Uversky, V. N., and Turoverov, K. K. *PLoS One* **5**(10), e15385 (2010).